On the Dynamics of the East African Jet. III: Arabian Sea Branch

PETER R. BANNON

Department of the Geophysical Sciences, The University of Chicago, Chicago, IL 60637

(Manuscript received 1 March 1982, in final form 25 June, 1982)

ABSTRACT

Barotropic simulations of the East African jet are extended to include the Arabian Sea branch of the flow and to allow for flow over the mountains of Africa. Large-scale mass source–sink forcing, present to the east of the model orography, drives the low-level circulation.

Many features of the southeast trades, cross-equatorial flow and southwest monsoon are simulated. Among them are the separation of the jet from the African highlands, a wind speed maximum over the Arabian Sea and a reinforcement of the southwest monsoon by the Arabian northerlies. Splitting of the jet over the Arabian Sea is not simulated.

Starting from a state of rest, a well-developed southwest monsoon is achieved in a week of simulated time. Inclusion of a prescribed Southern Hemisphere midlatitude disturbance excites a significant response in the cross-equatorial flow, even though flow is permitted over the African mountains. Downstream, the surges excite a response over both the Arabian Sea and the Bay of Bengal. The bay response lags that over the sea by one to two days and is a factor of 2 weaker. Despite the satisfaction of the necessary condition for barotropic instability, no signs of instability appear during the onset, surge or steady-state phases of the simulations.

1. Introduction

The structure of the low-level monsoon winds over the Indian Ocean during July consists of three elements: the southeast trades of the Southern Hemisphere; a strong narrow cross-equatorial flow over East Africa and the western edges of the Indian Ocean; and the southwest monsoon over the Arabian Sea. Together these components are often collectively called the East African or Somali jet (EAJ). The climatological structure of the EAJ is documented by Findlater (1977) and van de Boogaard (1977). The flow patterns for the summer of 1979 using Monsoon Experiment (MONEX) data are presented by Krishnamurti *et al.* (1980).

The scope of the author's earlier investigations (Bannon, 1979a,b; hereafter Part I and II, respectively) into the dynamics of the EAJ is limited to the region of the jet's formation and development over the south Indian Ocean and the east coast of Africa. Thus, the early studies focused on only two of the three major components of the flow: the southeast trades and the cross-equatorial jet. This study extends the analysis to include the Arabian Sea branch. The present numerical simulations are an improvement over the earlier works, in that 1) the assumption that the East African mountains are perfectly efficient in blocking the southeast trades is relaxed and the mountains here have finite height, and 2) the meridional domain of the model is quadrupled so that the artificial southern boundary at ~25°S is moved to ~60°S. Previous modeling efforts are reviewed by Hart (1977) and Anderson (1980).

In addition to confirming the results of the previous simulations over the south Indian Ocean, the present investigation addresses a number of aspects of the dynamics of the Arabian Sea branch:

a. Separation of the flow

Fig. 1 in Part I shows that the jet leaves the African coast at 10°N. An inviscid inertial boundary layer separates from a wall when the fluid depth vanishes (Hart, 1977); the Coriolis force alone is insufficient to deflect the flow eastward. Separation at a finite fluid depth can occur when the northward boundary current encounters southward flow (Anderson, 1976; Krishnamurti *et al.*, 1976). The presence of the Arabian northerlies associated with the monsoon heat low and of the eastward extension of the Ethiopian highlands appear crucial to the separation process. Differential surface drag between land and sea is also important in the eastward displacement of the jet core (Part I).

b. Wind speed maximum

After leaving the coast, the jet attains a relative maximum wind speed (~20 m s^{-1} at 1 km height) to the northeast of the tip of the Horn of Somalia. This feature could be a consequence of the reinforcement of the cross-equatorial flow, and/or of the re-

0022-4928/82/102267-12$07.00

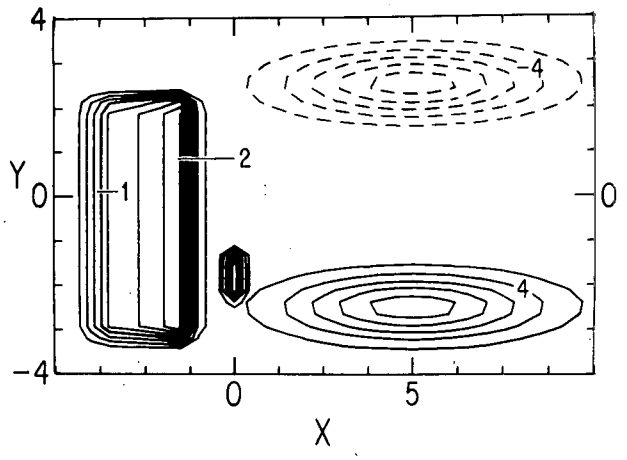

FIG. 1. Contour plot of the idealized bottom topography (km) of Africa and Madagascar with a contour interval (C.I.) of 250 m. Contour plot of the mass source (solid lines) and sink (dashed lines) have C.I. of 2 mm. All figures give horizontal distances in units of 1000 km.

duction in surface drag as the flow leaves the land and flows over the open ocean.

c. Jet bifurcation

Over the Arabian Sea, the jet axis splits (Findlater, 1977), one axis heads eastward for central India, while the second turns southeastward toward Sri Lanka. This behavior may result from *in situ* barotropic instability (Krishnamurti *et al.*, 1976) or synoptic disturbances over India (Cadet and Ovarlez, 1976). The bifurcation may also reflect interannual variations: during MONEX the southwest monsoon displayed no splitting; only the southern branch was present (Krishnamurti *et al.*, 1981).

d. Monsoon onset

As documented by Fieux and Stommel (1977), the onset of the southwest monsoon surface winds over the Arabian Sea usually (60% of the 25 years studied) consists of an abrupt (time interval less than one week) transition to strong winds over the entire region. Krishnamurti *et al.* (1981) document the monsoon onset during MONEX and suggest that barotropic instability of the southwest monsoon can explain the formation of the onset vortex.

e. Downstream influence of surges in the cross-equatorial flow

Variations in the strength of the cross-equatorial flow are documented by Findlater (1969, 1977). In particular, surges in the cross-equatorial flow due to Southern Hemisphere middle-latitude disturbances have been described observationally by Findlater (1969), Cadet and Desbois (1981), Rao and Haney (1982) and theoretically in Part II. However, the downstream influence of these surges over the Arabian Sea and Bay of Bengal could not be addressed in Part II. Anderson (1981) notes that linear theory predicts that such surges should be equatorially trapped. In nonlinear experiments without a northward cross-equatorial mean flow, he found that significant perturbation energy did not travel far across the equator for a pulse-like disturbance of period 2.4 days. Interhemispheric communication was only achieved by inertia–gravity waves. Here, low frequency (six-day period) sinusoidal disturbances are considered and a strong cross-equatorial mean flow is included.

The purpose of this investigation is to study these questions using a barotropic model of the low-level monsoon winds. The next section describes the physics of the model and the numerical techniques employed. Sections 3 and 4 report the results of the numerical simulations of the climatological and transient aspects of the EAJ, respectively. The paper concludes with a summary of the major results.

2. The model

a. Physics

The physical ingredients of the model are similar to those in Parts I and II. The equations of motion and of continuity describing the depth-averaged flow on an equatorial beta plane subject to Rayleigh damping, a reduced gravity (g'), and a mass source-sink distribution (Q) are

$$\frac{du}{dt} - \beta yv = -g'\frac{\partial h}{\partial x} - \frac{Ru}{D_0}, \tag{1a}$$

$$\frac{dv}{dt} + \beta yu = -g'\frac{\partial h}{\partial y} - \frac{Rv}{D_0}, \tag{1b}$$

$$\frac{dD}{dt} + D\left(\frac{\partial u}{\partial x} + \frac{\partial v}{\partial y}\right) = Q, \tag{1c}$$

where

$$\frac{d}{dt} \equiv \frac{\partial}{\partial t} + u\frac{\partial}{\partial x} + v\frac{\partial}{\partial y},$$

$\beta = 2.3 \times 10^{-11}$ m^{-1} s^{-1}, D is the fluid depth, $h = D + Z_B$ is the height of the free surface and Z_B is the variable bottom topography. The usual conventions hold.

The model orography used in the present study is shown in Fig. 1. The idealizations of the East African highlands and of Madagascar are similar to those in Parts I and II. Here, however, the assumption of a rigid western boundary at $x = 0$ is not made. The African mountains have a maximum height of 2.0 km and gradually decay westward to 1 km at $x = -2 \times 10^3$ km where they then drop precipitously to zero. This formulation models the Great Central Plateau and western escarpment of Africa. Fig. 2 pro-

vides a cross-section of the orography along the equator.

In order to allow for flow over the model mountains, the mean fluid depth should be greater than 2 km. A choice of 3 km is made here, based on the following considerations. Findlater's (1977) climatological cross section of the jet shows that the bulk of the cross-equatorial flow occurs below the 3 km height. The capping inversion often lies above the height of the African mountains at approximately the 3 km height level (Findlater, 1977).

The frictional parameterization using linear Rayleigh damping is identical to that in Parts I and II with $R = 1$ cm s^{-1}. Previously, the denominator for the last terms in (1a) and (1b) was the local instantaneous fluid depth $D(x, y, t)$. Here, however, $D_0(x, y) = D_{00} - Z_B(x, y)$ is used with $D_{00} = 3$ km. This linearization of the friction term makes the frictional decay time (D_0/R) take on the value of 3×10^5 s ≈ 3.5 days everywhere, except over the model orography where $D_0/R \geq 1.2$ days. This modification ensures that the damping of the flow over the Arabian Sea (where the fluid depth is small, see Fig. 3) is not unduly overestimated.

Another step taken to help produce a strong southwest monsoon is setting the reduced gravity g' equal to 1.20 m s^{-2}. Use of the original lower value of $g' = 0.60$ m s^{-2} limited the maximum model wind speeds to ~ 15 m s^{-1} over the Arabian Sea. Further increases in the strength of the forcing caused the model to blow up when the fluid depth vanished ($D \leq 0$) over the model monsoon low. The new choice of g' enabled a more vigorous circulation to be generated. Results with $g' = 0.60$ m s^{-2} exhibit no qualitative differences with those presented here, except that the necessary condition for barotropic instability was not achieved with $g' = 0.60$ m s^{-2}. Note that doubling the reduced gravity increases the equatorial deformation radius $(g'D/\beta^2)^{1/4}$ by only a factor of 1.2.

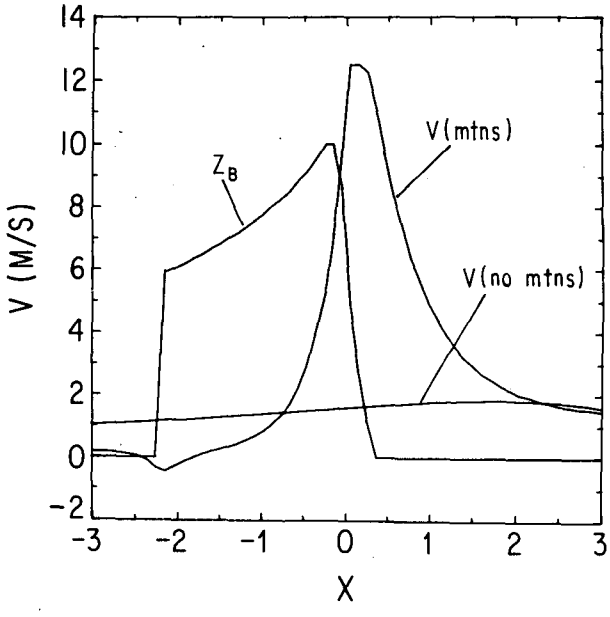

FIG. 2. Cross-equatorial flow as a function of longitude for the forcing of Fig. 1 with and without mountains. The model orography Z_B is also shown, such that 10 m s^{-1} = 2 km.

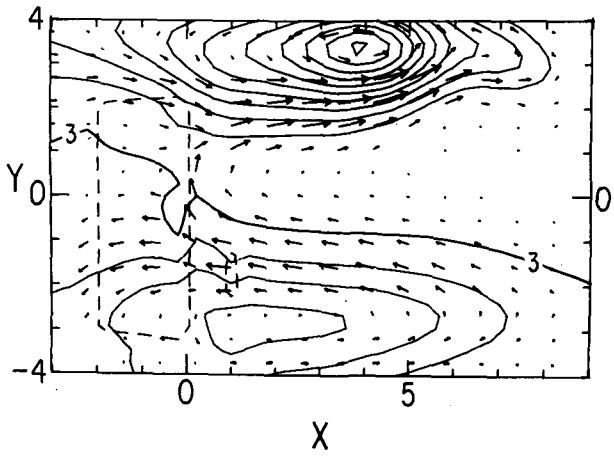

FIG. 3. Time average free surface height (km, C.I. = 200 m) and velocity vector field for the orography and forcing of Fig. 1. The maximum vector length (MV) corresponds to a speed of 25.6 m s^{-1}. The dashed line in this and subsequent figures is the 1000 m contour of the bottom topography.

The mass source term Q in the continuity equation (1c) simulates the flow forcing by the large-scale vertical circulation of the monsoon Hadley cell. A dipole distribution, antisymmetric about the equator, is assumed with a maximum of 1.12 cm s^{-1} at $(x, y) = (5000$ km, 2500 km) $\approx$ (90°E, 25°N). There is rising motion ($Q < 0$) in the Northern and subsidence ($Q > 0$) in the Southern Hemisphere. This distribution gives a simple representation of the monsoon Hadley cell. The forcing is not zonally symmetric but Gaussian in x with a half-width of 2.4×10^3 km. Fig. 1 shows the spatial distribution of the source–sink forcing Q. Model results are relatively insensitive to this zonal structure, provided it is large enough to strongly excite long Rossby waves.The sensitivity of the model results to the magnitude of Q, and to its latitudinal location and extent, is addressed in Section 3b. The possible time variation of the mass sink during the onset phase is not.

b. *Numerics*

The nonlinear model equations are solved numerically on a 24×10^3 km by 12×10^3 km domain, centered on the equator at $\sim$38°E. Impermeable zonal boundaries are present at $y = \pm 6 \times 10^3$ km; open boundaries lie at $x = \pm 12 \times 10^3$ km. The grid of 120×120 points is uniform in the y direction ($\Delta y = 100$ km) and stretched in the x direction (100 km $\leq \Delta x \leq$ 500 km). Because of the staggered dis-

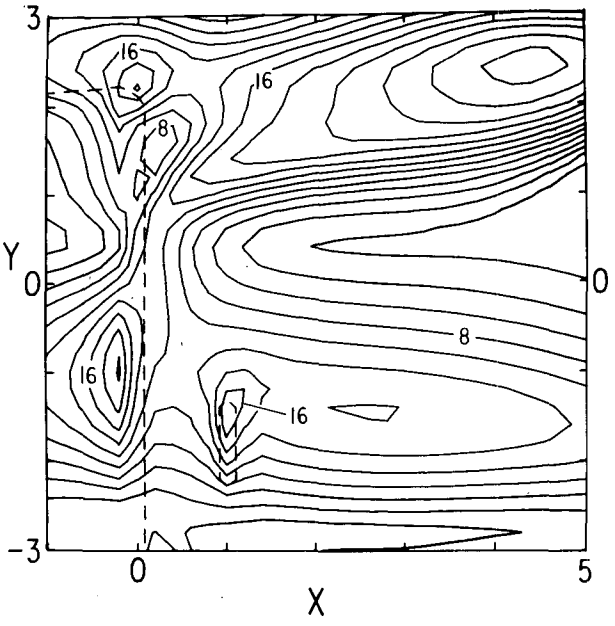

FIG. 4. Wind speed in m s^{-1} for the orography and forcing of Fig. 1. C.I. = 2 m s^{-1}.

tribution of the dependent variables, the effective resolution is 50 km in the region of interest.

The mathematical problem is treated as an initial-boundary-value one. The model is started from rest $(u, v, h) = (0, 0, 3$ km), and integrated forward in time for 50 model days, by which time an approximate steady state is achieved. The time integration follows Part I with a time step of 450 s. The horizontal boundary condition is $v = 0$ on the impermeable zonal boundaries. On the open east and west boundaries, $\partial u/\partial x$ (and $\partial v/\partial x$) are set to zero on outflow (inflow). The remaining computational boundary conditions are obtained by linear extrapolation. As the flow field is weak at $x = \pm 12 \times 10^3$ km, no computational difficulties with these boundary conditions arise. The remaining details of the numerical technique and the finite difference scheme are identical to those in Part I.

3. Climatological features of the simulation

a. *The basic experiment*

Starting from a state of rest, the numerical model is integrated for 50 model days with the forcing and topography shown in Fig. 1. After a spin-up period, a steady state is obtained over the last 10 days of simulation. The results presented in this section are based on the average over the last ten days of integration with a sampling interval of two days.

Fig. 3 displays the mean velocity vector field and free surface height over a portion of the computational domain. The display points for the flow vectors are not gridpoints. The wind speed for the flow is contour-plotted in Fig. 4. The three components of the low-level monsoon winds are present. The model southeast trades in the Southern Hemisphere have a peak speed of 14.1 m s^{-1}. There is a local intensification of the flow to 17.6 m s^{-1} to the northeast of Madagascar. Thereafter, the flow splits: one branch turns northward to form a narrow cross-equatorial flow; the other continues westward and crosses the model mountains of Africa. This westward branch has peak winds of 20.2 m s^{-1} centered at $(x, y) = (-200$ km, -1000 km) $\approx$ (36°E, 10°S) just downstream of the maximum height of the mountains at $x = 0$. This strong westward branch over Africa is shown in van de Boogaard's (1977) atlas to be at (30°E, 15°S) and have a maximum of 10 m s^{-1} at 850 mb. The June 850 mb climatology of Wright and Stubbs (1971) also shows a similar feature.

The cross-equatorial flow is better depicted in Fig. 2. The maximum meridional velocity is 12.5 m s^{-1}. This value is representative of the depth-averaged jet, but is low compared to the strength of the model trades and southwest monsoon. The jet is topographically bound to the east of the East African highlands with an eastern flank much broader than the western. The zonal structure and dynamics of the flow are the same as discussed in Part I, but here the fluid is permitted to flow over the mountain range. (The mountain peak is at 2.0 km while the free surface height is at $\sim$3.0 km.)

In the Northern Hemisphere, the model southwest monsoon has a broad wind-speed maximum of $\sim$20 m s^{-1} extending across the Arabian Sea. In agreement with observations, the southwest monsoon is swifter than the southeast trades while the cross-equatorial flow represents a relative minimum between the two. However, the simulated speed core over the sea is too far to the east and too far north of the separation point at $\sim$10°N. Furthermore, the model southwest monsoon is more westerly than observed and its meridional component is small. Fig. 3 shows that the southwest monsoon is reinforced more strongly by the Arabian northerlies than by the cross-equatorial flow. These discrepancies are re-examined in the next subsection.

Analysis of the horizontal divergence field $[(\partial u/\partial x) + (\partial v/\partial y)]$ (not shown) indicates there is convergence west of $x \approx 500$ km and divergence elsewhere over the Arabian Sea. This divergence field is consistent with the analyses of Gordon and Taylor (1975) and Rao *et al.* (1978) and with the observations of relatively cloudless skies (Ramage, 1971). Assuming a steady state, the continuity equation (1b) can be written as

$$\left(\frac{\partial u}{\partial x} + \frac{\partial v}{\partial y}\right) = \frac{1}{D}(Q - \mathbf{v}\cdot\nabla D). \tag{2}$$

Despite a specified sink ($Q < 0$), the flow's divergence is associated with strong flow down the pressure gra-

dient. The observed convergence over the eastern Arabian Sea is not simulated.

Fig. 3 also provides a contour plot of the height of the free surface (surface pressure). As expected, the pattern is dominated by the Mascarene high and monsoon low. The trough–ridge pressure distribution over the East African highlands is another realistic feature. Comparison with Fig. 2 of Part I is recommended. The heat lows over the Sahara and the Arabian peninsula are absent in Fig. 3. The maximum variation in the free surface height is ~2.7 km, corresponding to a surface pressure differential of ~30 mb.

Interestingly, the pressure extrema are displaced poleward and westward of the centers of maximum forcing Q at $(x, y) = (5000 \text{ km}, \pm 2500 \text{ km})$. These features are also present in the linear model of Gill (1980). The northward displacement arises because the vortices are generated by vortex stretching, which is proportional to βyQ and will have maxima poleward of the maximum value of Q. The westward displacement arises because the eastward and westward Fourier components of the forcing (Gaussian in x) will more strongly excite a westward response since all Rossby waves travel westward.

Unlike Gill, the cyclonic response is stronger than the anticyclonic. Since the nonlinear vortex stretching term is

$$(\beta y + \zeta)Q/D, \qquad (3)$$

the magnitude of the stretching is greater for cyclonic than anticyclonic circulations. Additionally, the greater westward displacement of the anticyclone can be explained by the fact that the mean flow is westward in the Southern Hemisphere and that the gravity wave speed $(g'D)^{1/2}$ is also greater where the fluid depth is larger.

b. *Sensitivity studies*

The results of the basic experiment indicate that the model simulates many features of the EAJ. Here the sensitivity of the model flow to changes in various parameters is determined. Specifically, variations in orography, friction and source distribution are addressed.

The African mountains are believed essential for the formation of the cross-equatorial jet. Fig. 2 compares numerical simulations with and without mountains. In either case the net cross-equatorial mass flux must be the same in order that a steady state be achieved. Fig. 2 shows that the presence of the mountains localizes this meridional mass flux into a jet stream topographically locked to the mountains. A measure of the blocking efficiency of the African mountains is

$$B = 1 - \hat{F}_{\text{mtn}}/\hat{F}_{\text{no mtn}}, \qquad (4)$$

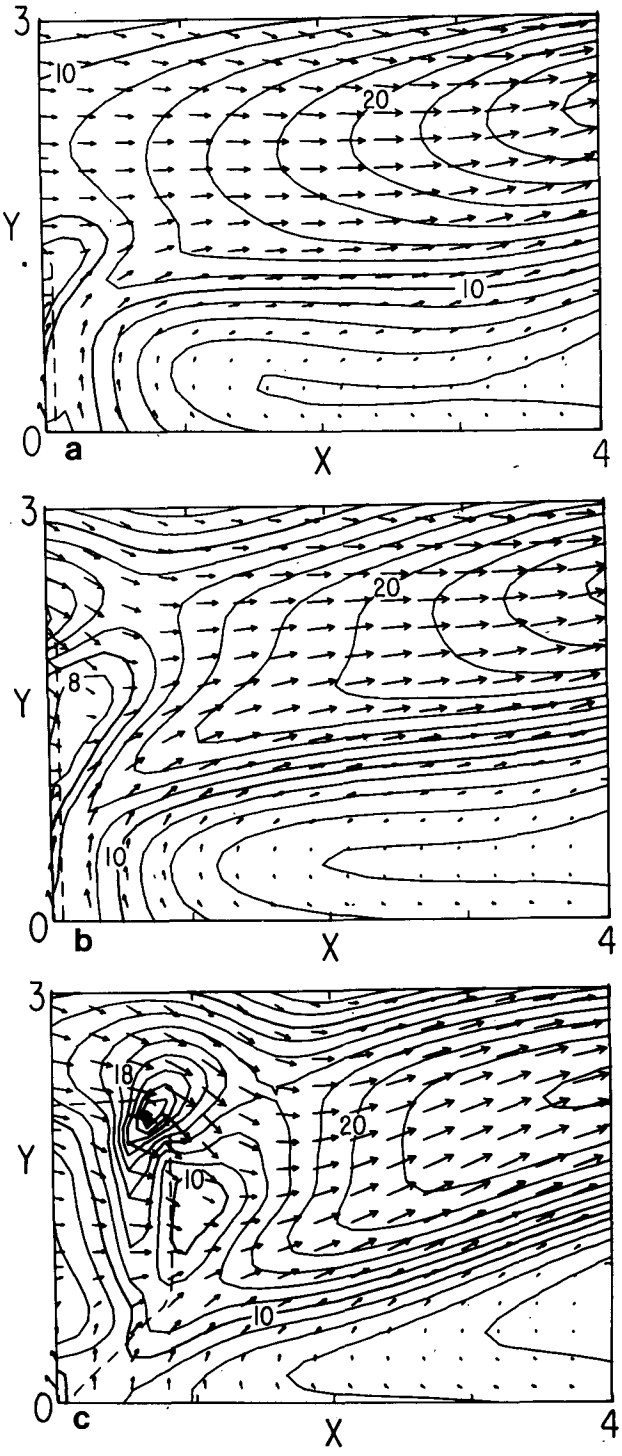

FIG. 5. Velocity vector field and wind speed (m s^{-1}) for three configurations of mountains: (a) no Arabian highlands; (b) Arabian highlands; (c) Arabian highlands plus the eastward extension of the Ethiopian mountains. MV is 26.0, 26.5 and 25.8 m s^{-1}, respectively. C.I. = 2 m s^{-1}.

where

$$\hat{F} = F(x = 0)/F(x = 2000 \text{ km})$$

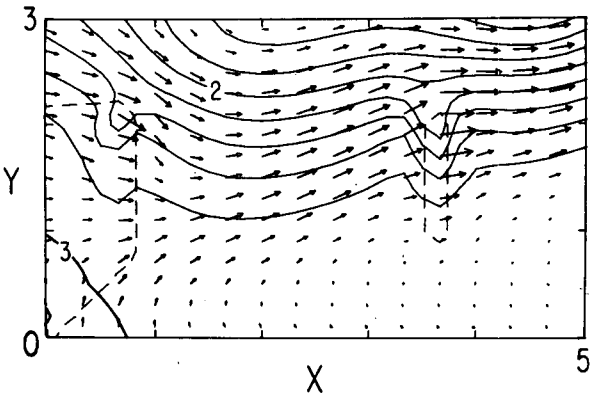

FIG. 6. Velocity vector field and free surface height (km) for an integration including the western Ghats. MV = 32.8 m s^{-1}. C.I. = 200 m.

is the ratio of the zonal mass flux F over the mountains to the flux incident 2000 km upstream. Here

$$F(x) = \int_{-y_0}^{0} u(x, y)D(x, y)dy$$

and y_0 = 2800 km. The blocking efficiency B is calculated to be only 0.40 so that 60% of the incident mass flux crosses over the mountains. The blocking efficiency is probably much larger in the real atmosphere, as the depth and strength of the southeast trades are overestimated by the model. The relatively low value obtained here helps explain the strength of the Arabian northerlies compared to the cross-equatorial flow in the basic experiment.

A series of experiments tests the response of the model flow to variations in the Ethiopian and Arabian highlands. The results are displayed in Fig. 5 for (a) a case without the Arabian highlands; (b) the basic experiment; and (c) a case including the eastward extension of the Ethiopian highlands. We define the separation point as that point along the 1 km topographic height contour where the meridional wind vanishes. Comparison of cases (a) and (b) indicates that the latitude of separation is independent of the length of the coastline, occuring at ~11°N in each simulation. The maximum cross-equatorial flow is weaker for the shorter coastline (11.4 m s^{-1}) and the blocking efficiency B is reduced slightly to 0.37. These results suggest that the mass flux required to compensate for the sink over India is, comparing (b and a), coming more from the South Indian Ocean directly, rather than indirectly after crossing Africa. The flow over the Arabian Sea is stronger and more southerly for the longer coastline case. The eastward extension of the Ethiopian highlands, (c), deflects the southerly cross-equatorial flow eastward sooner, again making the southwest monsoon stronger and more southerly. The cross-equatorial flow is slower but broader with the extension than without it. The extension intensifies the Arabian northerlies but separation remains at ~11°N. In each simulation the separation point is associated with intense cyclonic flow ($\partial v/\partial x > 0$, $\partial u/\partial y < 0$). This feature is reminiscent of the cyclonic eddy at the tip of Somalia, documented by Findlater (1971).

The effect of the Western Ghats of India is displayed in Fig. 6. The model Ghats are a north–south ridge with a peak height of 1.5 km and a Gaussian halfwidth of 150 km. Their presence causes a deflection of the flow northward and the creation of a wind speed maximum to the north of the range. Observations show that the deflection is southward. Only a weak symmetric trough is discernible. There is no wake of stationary Rossby waves as suggested by Gadgil (1977). The relevant nondimensional numbers are, in the notation of Bannon (1980): Rossby number $\epsilon \sim 1$–10; beta parameter $\hat{\beta} \sim 10^{-2}$; Ekman number $\gamma_R{}^2 \sim 10^{-2}$; and nondimensional mountain height $\mu \sim 0.5$. These values suggest a breakdown of quasi-geostrophic theory and only a weak beta effect for the model Ghats.

Another experiment tests the effect of a land–sea contrast in the frictional parameterization. The value of the Rayleigh drag coefficient over land is doubled in this run to 2 cm s^{-1}. The results are shown in Fig. 7. The increased drag over land has reduced the maximum wind speed over the African mountains from 20.2 to 13.4 m s^{-1}, more in agreement with observations. The blocking efficiency is increased substantially to 0.55 (from 0.41) and the southwest monsoon is more southerly and is fed more strongly by the cross-equatorial jet. The cross-equatorial flow (not

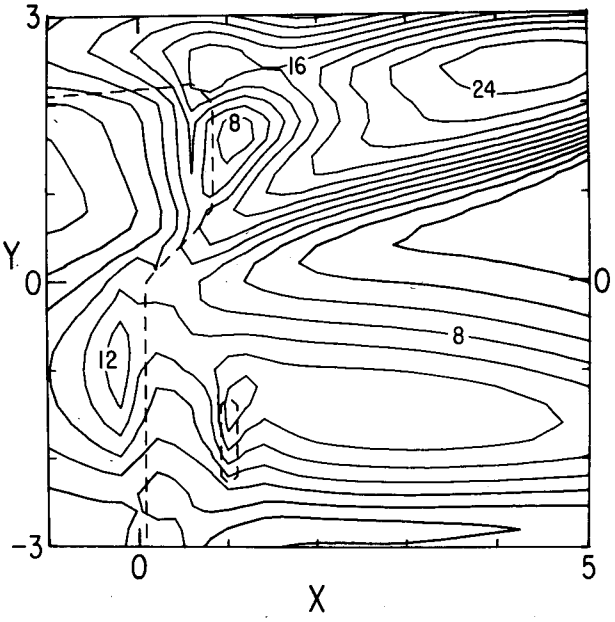

FIG. 7. Wind speed (m s^{-1}) for an integration with a land/sea contrast in bottom friction. C.I. = 2 m s^{-1}.

shown) has a structure like that displayed in Fig. 10 of Part I: a displacement of the jet maximum eastward to the coast. The structure of the flow downstream over the Arabian Sea is affected little by these variations in the upstream structure.

A final set of numerical experiments analyzes the sensitivity of the flow over the Arabian Sea to changes in the source–sink forcing Q. Fig. 8 displays the velocity vector field and wind speed contours for: a) Q halved; b) the halfwidth of Q halved in the Northern Hemisphere (NH); c) the Northern Hemisphere Q moved 10^3 km equatorward; and d) the NH sink split, half centered at ~25°N, half along the equator. A reduction in the forcing, case a), increases the blocking efficiency of the African mountains from 0.41 to 0.46 and produces a more southerly southwest monsoon. A relative wind speed maximum of 13 m s^{-1} appears over the central Arabian Sea. This feature agrees with observations and is not present in the earlier runs. Narrowing the sink, case b), has little effect on the flow. A southward displacement of the sink, case c), reduces the maximum winds from 26 to 18 m s^{-1} and shifts the jet core equatorward, more in line with the observations. This reduction in wind speed is consistent with the idea that vortex stretching is the dominant mechanism of flow generation. When the sink is split, case d), the winds are reduced in magnitude, and a relative maximum again appears over the central Arabian Sea. The split forcing does not cause the axis of maximum winds to bifurcate as observed in the Findlater climatology.

4. Transients

a. Monsoon onset

The question of the onset of the low-level winds over the Arabian Sea is analyzed by an examination of the spin-up phase of the numerical integration. Starting from a state of rest, the source–sink forcing is instantaneously turned on and the model is inte-

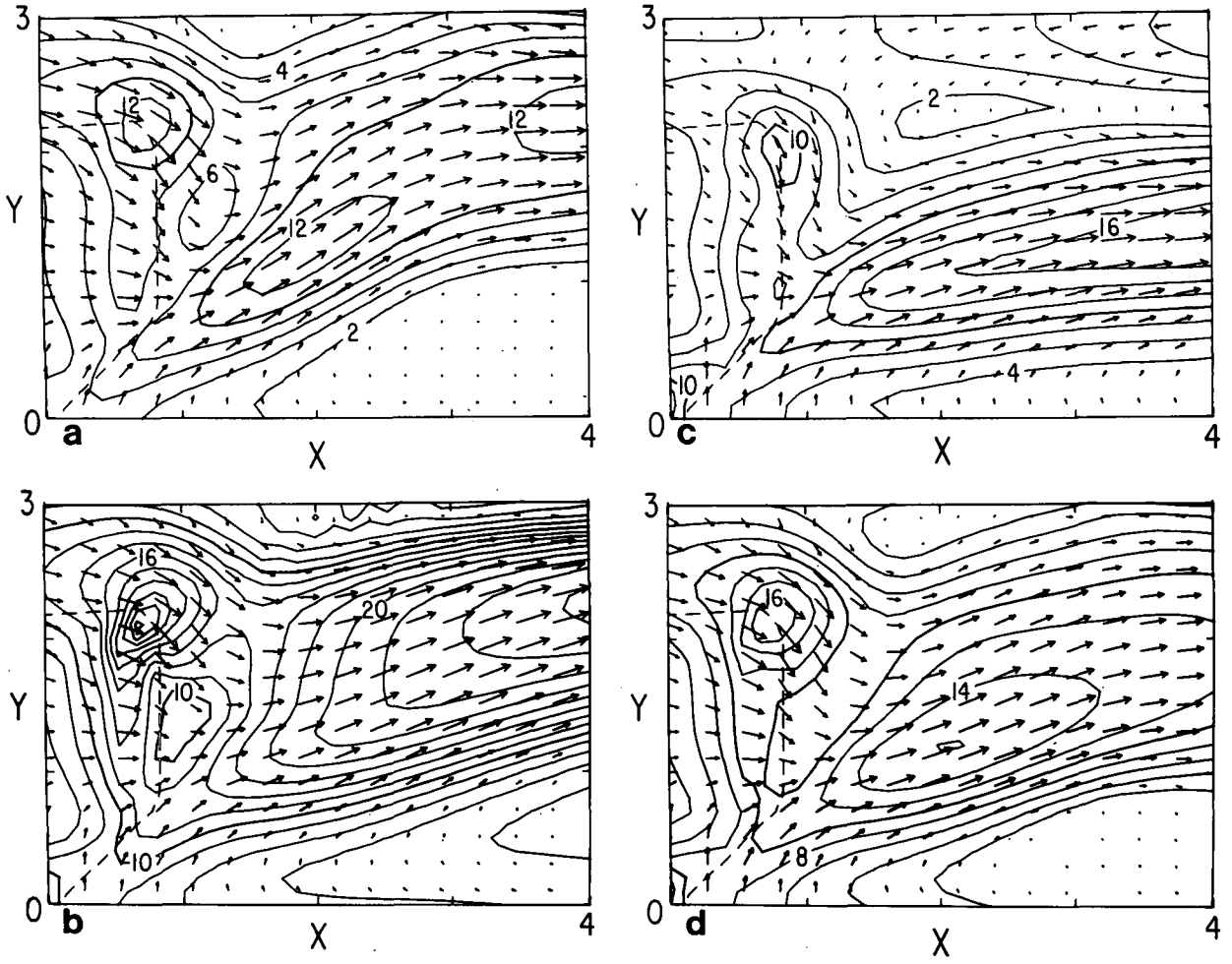

FIG. 8. Velocity vector field and wind speed (m s^{-1}) for four variations of the mass sink forcing of Fig. 1 with the orography of Fig. 5c: (a) forcing halved; (b) meridional halfwidth of forcing halved; (c) forcing centered at 15°N; (d) split forcing; half centered at 25°N and half at 0°. MV = 13.2, 25.6, 17.5 and 17.8 respectively. C.I. = 2 m s^{-1}.

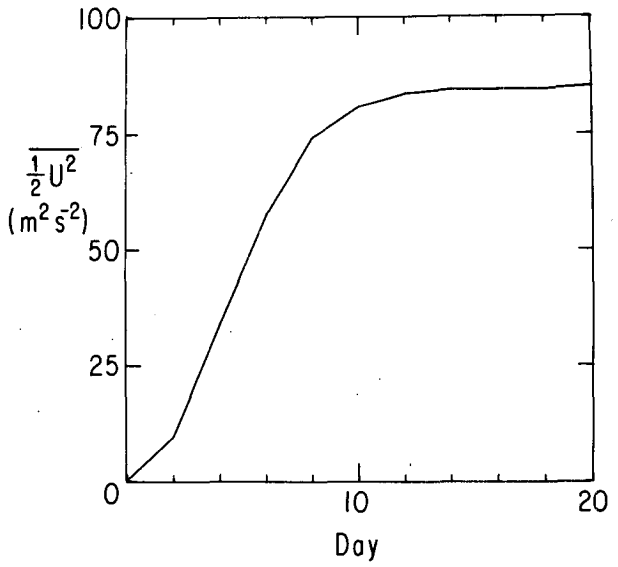

FIG. 9. Zonal kinetic energy per unit mass, $\frac{1}{2}u^2$, averaged over the Arabian Sea as a function of time.

grated forward in time. Krishnamurti *et al.* (1981) report that the mean zonal kinetic energy per unit over the Arabian Sea is small (<20 m^2 s^{-2}) before the 1979 onset, and so a state of rest is viewed as a simple pre-monsoonal flow state. As the following discussion suggests, the onset time is not believed to be an intrinsic property of the initial state.

Fig. 9 presents a plot of the zonal kinetic energy per unit mass, $\frac{1}{2}u^2$, averaged over the domain 1000 km $\leq x \leq$ 3000 km by 400 km $\leq y \leq$ 2000 km as a function of time. A fully developed southwest monsoon arises in two weeks time. This time development is similar to that reported by Krishnamurti *et al.* (1981) for the 1979 monsoon. However, the simulated onset is not as abrupt as that observed.

Comparison with other runs indicates that while the strength of the southwest monsoon is a function of the magnitude of the forcing, the abruptness of the onset is not. An objective measure of the onset period is defined here as the time it takes the zonal kinetic energy to rise from 10 to 90% of its peak value. From Fig. 9 this time is 6.6 days.

A physical interpretation of this onset time can be given following Lighthill (1969). The time for the formation of the southwest monsoon is the time it takes long Rossby waves to propagate into the Arabian Sea from the forcing region to the east. The zonal group velocity of these waves is $(g'D)^{1/2}(2m + 1)$ and westward, where $m = 1, 2, 3, \cdots$ is the meridional mode number. The onset time is

$$T \approx (2m + 1)L(g'D)^{-1/2}, \qquad (5)$$

where L is a characteristic distance to be traveled by the waves. For $L \approx 5 \times 10^3$ km, $g' = 1.20$ m s^{-2} and $D = 3$ km, $T \approx (2m + 1)$ days. This result is consistent with Fig. 9.

This theory indicates that the onset time varies by the inverse square root of the reduced gravity. Low resolution runs with $g' = 0.60$ m s^{-2} have onset times of $\sim$10.0 days. Here 10 days/6.6 days $\approx 1.5 \approx 2^{1/2}$, in good agreement with theory.

b. *Jet surges*

The presence of midlatitude disturbances in the Southern Hemisphere is simulated by a sinusoidal distribution of mass sources and sinks along $y = -3.0 \times 10^3$ km with a zonal wavelength of 6×10^3 km, a period of six days and eastward phase propagation. The forcing has a Gaussian distribution in y with a standard deviation of 10^3 km and an amplitude of 1.0 cm s^{-1}. [Stronger forcing caused the fluid depth to vanish ($D < 0$) over the Ethiopian highlands.] This forcing is instantaneously switched on at day 30 of the basic experiment. The model is run forward in time for three cycles (18 days). The following results are for the third cycle.

The response of the cross-equatorial flow to this transient forcing is shown in Fig. 10 for cases with and without the orography of Fig. 1 (the basic experiment). The deviation of the meridional wind along the equator from its average over the last cycle is plotted. The no-mountain case has a magnitude of 0.30 m s^{-1} compared to that of the meridional velocity excited at $y = -3.0 \times 10^3$ km of 2.5 m s^{-1}. This weak response for eastward-propagating modes is consistent with the analyses of Bennett and Young (1971) and Part II. The eastward phase propagation of the response in Fig. 10 indicates that the generation of the spurious anti-Kelvin wave solution is, if existent, negligible.

The presence of the mountain enables a stronger equatorial response to develop. The magnitude is 1.5 m s^{-1}, indicating an intensification factor $I = 1.5/2.5 = 0.60$ ($I \equiv$ ratio of the magnitudes along the equator and a southern latitude; see Part II). The case of lateral forcing treated in Part II yields an intensification factor $I = 1.0$. The difference arises due to the difference in the forcing and in the finite height of the African mountains, enabling flow over the highlands.

The equatorial response is greater to the east of the mountains than to the west. The phase relation is such that the meridional flow is in opposite directions on either side of the highlands. The phase of the response is such that the maximum cross-equatorial flow (Day 1) occurs when the center of the synoptic high pressure cell along $\sim$30°S lies at $x = 0$. Thus, the maximum response occurs 1.5 days after the maximum pumping up the Mozambique Channel. These results are consistent with the studies of Part II and Bannon (1981). Unlike Part II, the response

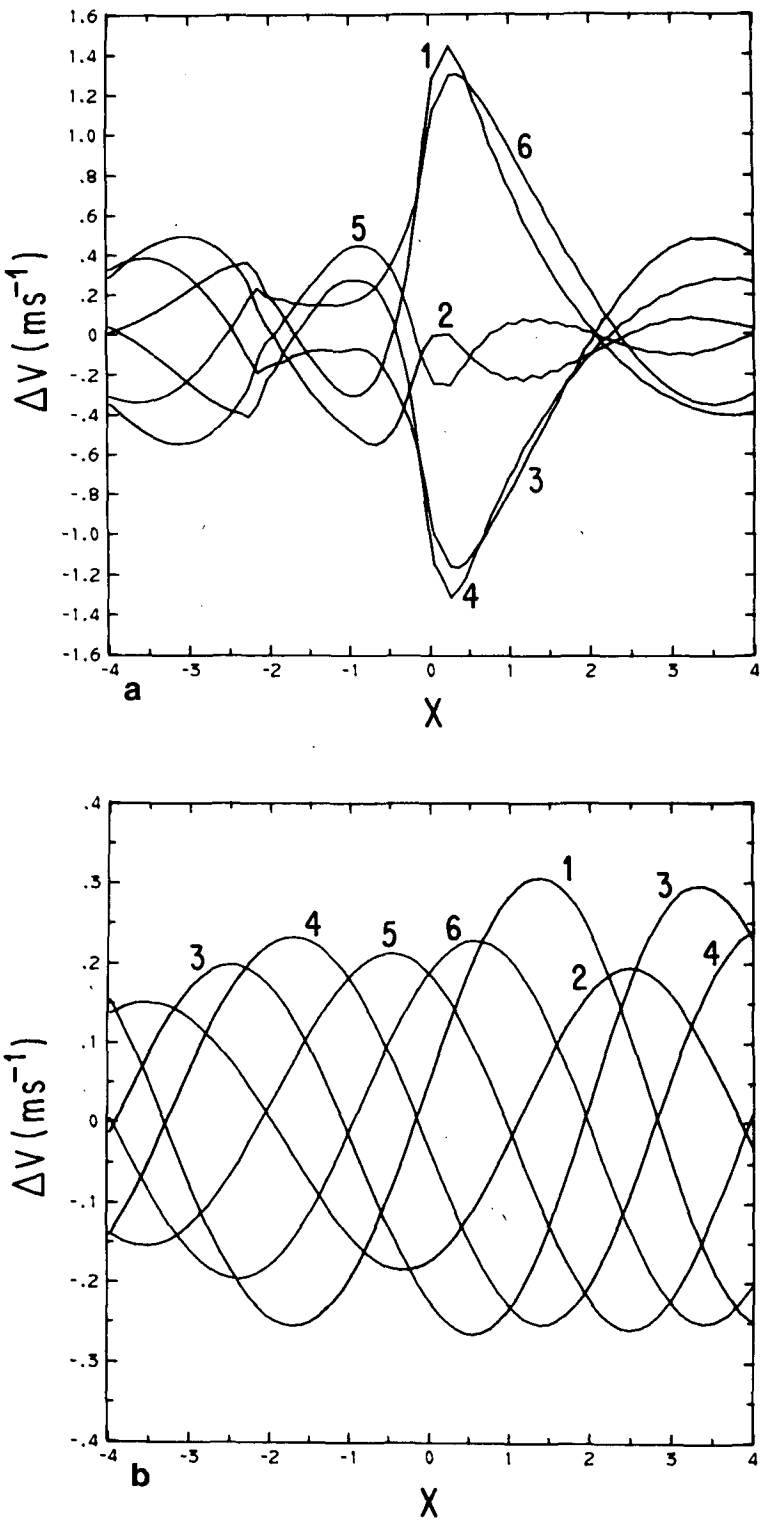

FIG. 10. Response of the cross-equatorial flow to Southern Hemisphere forcing as a function of longitude for cases (a) with, and (b) without, mountains. The deviation from the time mean over the third cycle of the forcing with a period of six days is plotted. Curve labels are in days. Day 1 refers to the time when the midlatitude synoptic high pressure is centered at $x = 0$.

TABLE 1. Influence of cross-equatorial surge over the Arabian Sea.

	Mountains		No mountains	
Day	$\langle KE \rangle$ ($m^2 s^{-2}$)	$\langle h \rangle$ (m)	$\langle KE \rangle$ ($m^2 s^{-2}$)	$\langle h \rangle$ (m)
1	+3.7	+16	0.0	−5
2	+0.5	+12	0.5	0
3	−2.6	−2	0.2	+2
4	−3.7	−14	−0.4	+2
5	−1.2	−15	−0.4	+1
6	+3.2	+2	0.2	+2

east of the mountains is a standing rather than propagating wave.

The downstream influence of the surges in the cross-equatorial flow is assessed objectively in Table 1 which tabulates the temporal variation over the Arabian Sea of the kinetic energy per unit mass $\langle KE \rangle = \langle (u^2 + v^2)/2 \rangle$, and of the free surface height $\langle h \rangle$ from their mean values during the third cycle. Here the angle brackets denote the horizontal average over the domain $1000 \leq x \leq 3000$ km and $400 \leq y \leq 2000$ km. Table 1 includes results for the mountain and no-mountain cases. The latter acts as an experimental control and measures the background noise associated with the Southern Hemisphere forcing, which arises due to the numerical approach (boundary conditions, etc.). A periodic response is clearly present in the mountain case: an increase in the kinetic energy and surface pressure over the Arabian Sea is in-phase with an intensification of the cross-equatorial flow. The magnitude of the response is greater by a factor of 3–4 than the control case. It is therefore concluded that the response in the mountain case is significant.

A similar analysis for the Bay of Bengal region is presented in Table 2. The areal average is taken over the domain $4000 \leq x \leq 6000$ km and $400 \leq y \leq 2000$ km. The response for the mountain case is 2–3 times stronger than the control; the kinetic energy and surface pressure lag the intensification of the cross-equatorial flow by 1–2 days. These results suggest that the downstream influence of surges in the cross-equatorial flow can extend into the region of the Bay of Bengal.

TABLE 2. Influence of cross-equatorial surge over the Bay of Bengal.

	Mountains		No mountains	
Day	$\langle KE \rangle$ ($m^2 s^{-2}$)	$\langle h \rangle$ (m)	$\langle KE \rangle$ ($m^2 s^{-2}$)	$\langle h \rangle$ (m)
1	−0.4	+4	−0.6	−5
2	+1.8	+8	−0.1	0
3	+1.9	+1	+0.5	+4
4	+0.2	−4	+0.5	+3
5	−1.7	−8	+0.1	+1
6	−1.8	+1	−0.2	−1

c. *Flow stability*

A final topic is the stability of the simulated flow. During the numerical integration of each of the cases discussed, no signs of flow instability were exhibited, either during the onset, steady state or surge periods. However, inspection of the ten-day mean zonal wind averaged over the zone $1000 \leq x \leq 3000$ km indicates that the necessary condition for barotropic instability was achieved for some of the integrations. Fig. 11 provides an example from the basic experiment.

The relatively broad zonal jet has a maximum of 18.9 m s^{-1} and a relative minimum of absolute vorticity $\beta y - (\partial u/\partial y)$, at ~11°N, south of the jet maximum. These features are consistent with the MONEX observations presented by Krishnamurti *et al.* (1981), particularly the 13 June case of their Fig. 13. For that occasion they predict a growth rate for the disturbance of 1×10^{-6} s^{-1}. Their inviscid barotropic numerical simulation documents the creation of the onset vortex as the result of barotropic instability. One possible explanation for the lack of vortex formation in the present study is the presence of bottom friction with a decay rate of 3.3×10^{-6} s^{-1}. Friction appears adequate to suppress any instabilities here.

Another possible instability mechanism is inertial instability. The profile of Fig. 11 has negative absolute vorticity poleward from the equator to 4°N. Again, no signs of instability manifested themselves.

5. Conclusions

A barotropic primitive equation model with orography and bottom friction is used to simulate the low-level monsoon winds. The idealized bottom to-

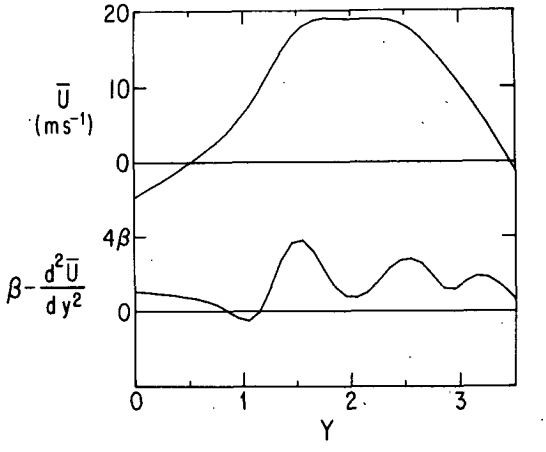

FIG. 11. Mean zonal wind over the Arabian Sea as a function of latitude for the configuration of Fig. 1, and the corresponding gradient of the absolute vorticity, $\beta - (d^2\bar{u}/dy^2)$.

pography is everywhere less than the height of the free surface, enabling flow over and around the African mountains. A large-scale distribution of mass sources and sinks drives the flow. All forcing lies well to the east of the model Africa. The three major components of the winds (i.e., the southeast trades, the cross-equatorial jet and the southwest monsoon) are simulated.

Results of numerical experiments indicate the important role of the local topography. The mountains of East Africa are crucial to the western intensification of the cross-equatorial flow. Approximately 40–55% of the Southern Hemisphere easterlies are deflected meridionally by the model African mountains. Variations in the Arabian and Ethiopian highlands are reflected in the jet structure. A long straight mountain ridge in the Northern Hemisphere produces a stronger cross-equatorial flow than a short ridge. However, the separation of the jet is independent of the length of the ridge, occurring at ~11°N. Inclusion of the eastward extension of the Ethiopian highlands produces a slower and broader cross-equatorial flow, and a stronger and more southerly southwest monsoon. The separation point of the flow is insensitive to changes in bottom topography and frictional parameterization; it always occurs at ~11°N. This finding is consistent with the study of Parsons (1969). The presence of the western Ghats of India does not lead to an appreciable lee trough in the Bay of Bengal.

The simulated wind speed patterns exhibit many realistic features including relative maxima near Madagascar, over Zambia/Zimbabwe, and off the Horn of Somalia over the Arabian Sea and a minimum along the equator. The simulated southwest monsoon is stronger than the southeast trades. The former appears to be reinforced by the dry Arabian northerlies and not to be the result of the separation process or of a land/sea contrast in the frictional parameterization. Splitting of the simulated Arabian Sea wind maxima into two branches does not occur for a variety of model orographies and mass sink distributions. The observed splitting is therefore believed to arise from synoptic and/or climatological variations of the large-scale forcing and not to be an intrinsic property of the southwest monsoon. Though the flow satisfied the necessary condition for barotropic instability, no instabilities arise. (The bottom friction, with decay rate 3.3×10^{-6} s^{-1}, is apparently adequate to suppress any unstable disturbances.)

The question of the onset of the southwest monsoon is examined during the model spin-up. Starting from a state of rest, a well-developed southwest monsoon is achieved after 7–10 days of simulated time. The source–sink forcing is constant with time during this spin-up. The duration of this onset is consistent with the time it takes long Rossby waves, generated in the region of forcing to the east, to propagate westward into the Arabian Sea. No signs of barotropic instability or vortex generation appear during the model spin-up. The discrepancy of this last result with those of Krishnamurti *et al.* (1981) may lie in the use of bottom friction here and its absence in Krishnamurti *et al.* Further research should address this point.

The downstream influence of surges in the cross-equatorial flow is examined in a final set of numerical experiments. Here, the surges are generated along 30°S by an eastward-propagating zonally sinusoidal distribution of mass sources and sinks which crudely represent the low-level forcing of baroclinic disturbances of the Southern Hemisphere. This forcing generates a significant equatorial response only with orography present and despite the fact that the model African mountains are of finite height. The equatorial response is greater on the eastern side of the mountain chain and 180° out of phase with that on the western side. Downstream, their influence extends into the Arabian Sea and to the Bay of Bengal. Surges in the cross-equatorial flow occur one and a half days (a quarter period) after strong northward pumping along southern Africa and are simultaneously associated with a pressure rise and an increase in kinetic energy over the Arabian Sea. The Bay of Bengal response lags that over the Arabian Sea by one to two days and is a factor of two weaker. As the group velocity of mixed Rossby–gravity and Rossby waves at six day period are small (≤ 2 m s^{-1}), these results suggest that the mean background flow, absent in the study of Anderson (1981), is advecting the surges downstream. As during the model spin-up, no signs of barotropic instability appear.

Inherent in the simplicity of the present model are several important limitations. The barotropic approach implies that the model can provide no information on the vertical structure of the jet and that the baroclinic forcing in regions of strong thermal gradients (e.g., the coasts of Somalia and Arabia) is precluded. As the strength of the monsoon Hadley cell (Q) is prescribed, its variation during the onset period or surge conditions could not be studied. For example, a surge of warm moist air across the equator may intensify the monsoon circulation. Specification of the stratification (g') eliminates an investigation into the dynamics of the monsoon inversion. The downstream thickening of the inversion by mechanical and buoyancy driven turbulence would slow the jet and raise the inversion base. This process could explain the low-level convergence observed over the eastern Arabian Sea but not simulated in the present calculations. These limitations will hopefully be addressed in future research.

Acknowledgments. This research was supported by the Louis Block Fund of the University of Chicago and by the National Science Foundation under Grant

No. ATM-8026790. The numerical computations were performed at the National Center for Atmospheric Research which is sponsored by the National Science Foundation.

REFERENCES

Anderson, D. L. T., 1976: The low-level jet as a western boundary current. *Mon. Wea. Rev.*, **104,** 907–921.

——, 1980: Orographically controlled cross-equatorial flow. *Orographic Effects in Planetary Flows*, R. Hide, Ed., *GARP Publ. Ser.*, No. 23, 317–355.

——, 1981: Cross-equatorial waves, with applications to the low-level East-African jet. *Geophys. Astrophys. Fluid Dyn.*, **12,** 267–284.

Bannon, P. R., 1979a: On the dynamics of the East African Jet. Part I. Simulation of mean conditions for July. *J. Atmos. Sci.*, **36,** 2139–2152.

——, 1979b: On the dynamics of the East African jet. II. Jet transients. *J. Atmos. Sci.*, **36,** 2153–2168.

——, 1980: Rotating barotropic flow over finite isolated topography. *J. Fluid Mech.*, **101,** 281–306.

——, 1981: Synoptic-scale forcing of coastal lows: forced double Kelvin waves in the atmosphere. *Quart. J. Roy. Meteor. Soc.*, **107,** 313–327.

Bennett, J. R., and J. A. Young, 1971: The influence of latitudinal wind shear upon large-scale wave propagation into the tropics. *Mon. Wea. Rev.*, **99,** 202–214.

Cadet, D., and M. Desbois, 1981: A case study of a fluctuation of the Somali jet during the Indian summer monsoon. *Mon. Wea. Rev.*, **109,** 182–187.

——, and H. Ovarlez, 1976: Low-level air flow circulation over the Arabian Sea during the summer monsoon as deduced from satellite-tracked superpressure balloons. Part I. Balloon trajectories. *Quart. J. Roy. Meteor. Soc.*, **102,** 805–816.

Fieux, M., and H. Stommel, 1977: Onset of the southwest monsoon over the Arabian Sea from marine reports of surface winds: Structure and variability. *Mon. Wea. Rev.*, **105,** 231–236.

Findlater, J., 1969: A major low-level air current near the Indian Ocean during the northern summer. *Quart. J. Roy. Meteor. Soc.*, **95,** 362–380.

——, 1971: The strange winds of Ras Asir. *Meteor. Mag.*, **100,** 46–54.

——, 1977: Observational aspects of the low-level cross-equatorial jet stream of the western Indian Ocean. *Pure Appl. Geophys.*, **115,** 1251–1262.

Gadgil, S., 1977: Orographic effects on the southwest monsoon: A review. *Pure Appl. Geophys.*, **115,** 1413–1430.

Gill, A. E., 1980: Some simple solutions for heat-induced tropical circulation. *Quart. J. Roy. Meteor. Soc.*, **106,** 447–462.

Gordon, A. H., and R. C. Taylor, 1975: Computations of surface layer air parcel trajectories and weather in the oceanic tropics. *International Indian Ocean Expedition, Meteor. Monogr.*, No. 7, University of Hawaii Press, 112 pp.

Hart, J. E., 1977: On the theory of the East African low level jet stream. *Pure Appl. Geophys.*, **115,** 1263–1282.

Krishnamurti, T. N., Y. Ramanathan, P. Ardanuy, R. Pasch and P. Greiman, 1980: Quick Look "Summer MONEX Atlas." Part III: Monsoon Depression Phase. Florida State University Rep., No. 80-8, 135 pp.

——, P. Ardanuy, Y. Ramanathan and R. Pasch, 1981: On the onset vortex of the summer monsoon. *Mon. Wea. Rev.*, **109,** 344–363.

——, J. Molinari and H. L. Pan, 1976: Numerical simulation of the Somali jet. *J. Atmos. Sci.*, **33,** 2350–2362.

Lighthill, M. J., 1969: Dynamic response of the Indian Ocean to the onset of the southwest monsoon. *Phil. Trans. Roy. Soc. London*, **A265,** 45–92.

Parsons, A. T., 1969: A two-layer model of Gulf Stream separation. *J. Fluid Mech.*, **39,** 511–528.

Ramage, C. S., 1971: *Monsoon Meteorology.* Academic Press, 296 pp.

Rao, G. V., and J. L. Haney, 1982: Kinematic and thermal structures of two surges of flow in the northern Mozambique channel area. *Quart. J. Roy. Meteor. Soc.*, **108** (in press).

——, H. M. E. van de Boogaard and W. C. Bolhofer, 1978: Further calculations of sea level air trajectories over the equatorial Indian Ocean. *Mon. Wea. Rev.*, **106,** 1465–1475.

van de Boogaard, H., 1977: The mean circulation of the tropical and subtropical atmosphere—July. NCAR Tech. Note NCAR/TN-118 + STR., 48 pp.

Wright, P. B., and M. W. Stubbs, 1971: Circulation patterns at 850, 700, 500 and 200 millibars over the eastern hemisphere from 40°N to 40°S during May and June. U.K. Meteor. Office *Geophys. Mem.*, No. 114, 40 pp.